

# **Clarifying the role of the lattice degree of freedom in the canonical metal to insulator transition in $V_2O_3$**

Ethan Roch Alain Fletcher

A thesis submitted to the faculty of

Brigham Young University

In partial fulfillment of the requirements for the degree of

Bachelor of Science

Dr. Benjamin Frandsen, Advisor

Department of Physics and Astronomy

Brigham Young University

April 22, 2021

Copyright © 2021 Ethan Roch Alain Fletcher

All Rights Reserved

## **ABSTRACT**

V<sub>2</sub>O<sub>3</sub> is an important material for the study of Mott insulators and other strongly correlated electron systems. Despite decades of research, a complete understanding of the metal-insulator transition in V<sub>2</sub>O<sub>3</sub> has not been conclusively established. Here, we present comprehensive atomic and magnetic pair distribution function (PDF) analyses of V<sub>2</sub>O<sub>3</sub> using both x-ray and neutron total scattering measurements, shedding new light on the mechanism of the transition from the point of view of short-range structural and magnetic correlations on both sides of the transition. We observe an abrupt structural transition with no hint of short-range monoclinic distortions above the transition temperature. This lack of structural fluctuations above the transition contrasts with the known presence of magnetic fluctuations in the high-temperature state, suggesting that the lattice degree of freedom plays a secondary role behind the spin degree of freedom in the transition mechanism.

### **KEYWORDS:**

Mott Insulator; metal-to-insulator transition; monoclinic; rhombohedral; local structure; magnetic correlations

# Acknowledgements

No words can express how grateful I am for my parents, who nurtured my love for physics, despite never understanding where it came from, and helped me develop to become the man I am today and still can become.

Ashley and Helena, y'all have my thanks, for always being willing to listen to my musings about my research and its implications. Y'all underestimate how much it helped me progress in my understanding of what I was doing.

Ben, you have been invaluable as my advisor. I am forever indebted to you for your endless patience with my many questions, musings, and the numerous times I randomly barged into your office to bug you. Thank you for giving me the chance to find what I want to dedicate my life to: condensed matter physics! Your guidance and support mean more to me than you could ever know.

I am grateful to the faculty of the physics department here at BYU, for their empathy, compassion, and the slew of opportunities they gave me as an undergraduate. I hope I can repay the favor someday.

To all my other friends and mentors, both here at the Y and elsewhere, thank you for being part of this wonderful journey.

# Table of Contents

<b>Table of Contents</b> .....	<b>4</b>
<b>List of Figures</b> .....	<b>6</b>
<b>List of Tables</b> .....	<b>8</b>
<b>Chapter 1 Introduction</b> .....	<b>10</b>
1.1 Mott Insulators .....	10
1.2 Vanadium (II) Oxide (III) .....	11
1.3 Motivation.....	12
1.4 Previous Work .....	13
1.5 Scientific question addressed by this research.....	15
1.6 Summary of results .....	16
1.7 Overview.....	16
<b>Chapter 2 Procedural Methods</b> .....	<b>17</b>
2.1 Sample Acquisition and Characterization.....	17
2.2 Experimental Procedure and Data collection.....	17
2.2.1 Experimental preparation.....	18
2.2.2 Data collection .....	18
2.3 Pair Distribution Function (PDF).....	20

2.3.1 Atomic PDF .....	21
2.3.2 Magnetic pair distribution function (mPDF) analysis .....	23
2.4 Data Analysis .....	25
2.4.1 PDFgui .....	25
2.4.2 PDF Refinement in diffPy .....	27
2.4.3 Shortcomings of PDFgui and diffPy .....	27
2.4.4 diffPy.mpdf Package .....	28
2.4.5 Shortcomings of diffPy.mpdf .....	29
<b>Chapter 3 Results and Conclusions .....</b>	<b>30</b>
3.1 V <sub>2</sub> O <sub>3</sub> Results and Analysis .....	30
3.1.1 Atomic PDF Fit Results .....	30
3.1.2 Magnetic PDF Analysis .....	31
3.1.3 Analysis of V <sub>2</sub> O <sub>3</sub> Results .....	41
3.2 Future Work .....	43
3.3 Summary and Conclusion .....	44
<b>Bibliography .....</b>	<b>45</b>

# List of Figures

<b>Figure 1.1</b> V <sub>2</sub> O <sub>3</sub> phase diagram.....	11
<b>Figure 1.2</b> Configurations of the monoclinic and rhombohedral crystallographic symmetries....	12
<b>Figure 1.3</b> Visualization of the triangular symmetry between vanadium atoms .....	14
<b>Figure 1.4</b> Resistivity/Bond length vs. Temperature .....	15
<b>Figure 2.1</b> Visualization of the pair distribution function.....	22
<b>Figure 2.2</b> Sample PDF fit .....	26
<b>Figure 3.1</b> Atomic PDF fit of rhombohedral neutron data at 300 K.....	31
<b>Figure 3.2</b> Atomic PDF fit of rhombohedral x-ray data at 303.84 K.....	32
<b>Figure 3.3</b> Atomic PDF fit of monoclinic x-ray and neutron data at ~100 K.....	33
<b>Figure 3.4</b> Waterfall plot of temperature series of atomic PDF x-ray data.....	34
<b>Figure 3.5</b> Low- <i>r</i> features in the atomic PDF x-ray data .....	35
<b>Figure 3.6</b> Waterfall plot of temperatures series of atomic PDF neutron data .....	36
<b>Figure 3.7</b> Low- <i>r</i> features in the atomic PDF neutron data .....	37
<b>Figure 3.8</b> Vanadium-vanadium bond lengths vs. temperature .....	39
<b>Figure 3.9</b> Convergence of the monoclinic phase to the rhombohedral phase .....	40
<b>Figure 3.10</b> mPDF fits at 100 K and 150 K .....	41
<b>Figure 3.11</b> Temperature evolution of the best fit ordered moment .....	42



# List of Tables

**Table 2.2.1** Qdamp and Qbroad values per fitting range .....18



# Chapter 1

## Introduction

In this chapter, I will address the topic of Mott insulators and the interesting nature of the transition that occurs in  $V_2O_3$  in preparation for later discussion on the mechanism behind the metal to insulator transition observed in  $V_2O_3$ .

### 1.1 Mott Insulators

Mott insulators are a class of materials that, under conventional band theory, would be classified as conductors. However, they instead demonstrate insulating properties, which are largely due to strong, local electron-electron correlations in the lattice. These materials are not necessarily uniquely insulating. They can become conductors under certain circumstances. For example, some Mott insulators become conductors at sufficiently high temperature, under the application of pressure, or through doping to change the chemical composition of the material.

Although the importance of strong electron-electron repulsion is widely recognized as the key ingredient for the Mott insulating transition, the underlying mechanism is not yet fully understood. However, common features have been observed in many Mott insulators, including the presence of antiferromagnetic ordering, suggesting that magnetism is closely related to Mott physics.

### 1.2 Vanadium (II) Oxide (III)

$V_2O_3$  is already an interesting material due to its classification as a Mott insulator. What makes it more of an interesting study is the fact that the transition it undergoes is three-fold rather than singular, as illustrated by the phase diagram in Figure 1.1.

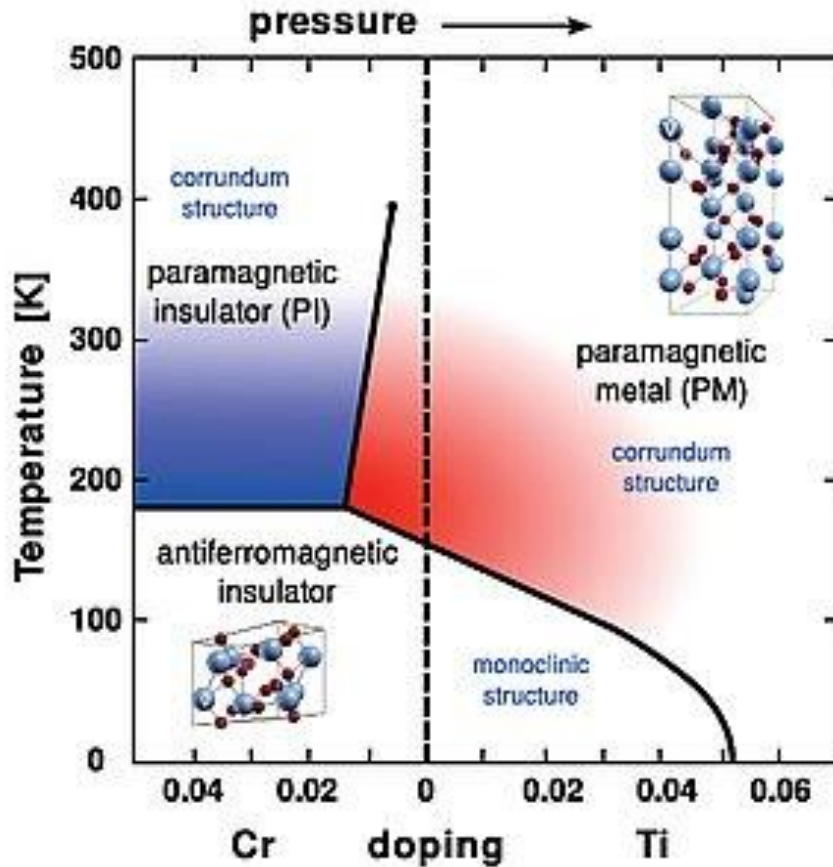


**Figure 1.1:** This is a phase diagram illustrating the different changes that  $V_2O_3$  undergoes once it reaches the transition temperature. It is necessary to note that our substance was not doped, so along the doping axis, all assumptions are made at the point where the doping is zero. Source: <https://www.physik.uni-wuerzburg.de/for1162/projects/p8/>, accessed March 2019.

In our experiment, the three-fold transition occurs between 155 K and 160 K. At temperatures above the transition, which we will denote the high temperature phase, the average crystallographic symmetry is rhombohedral. At temperatures below the transition, the low

temperature phase, the average crystallographic symmetry is rhombohedral. These symmetries are represented in figure 1.2 below.

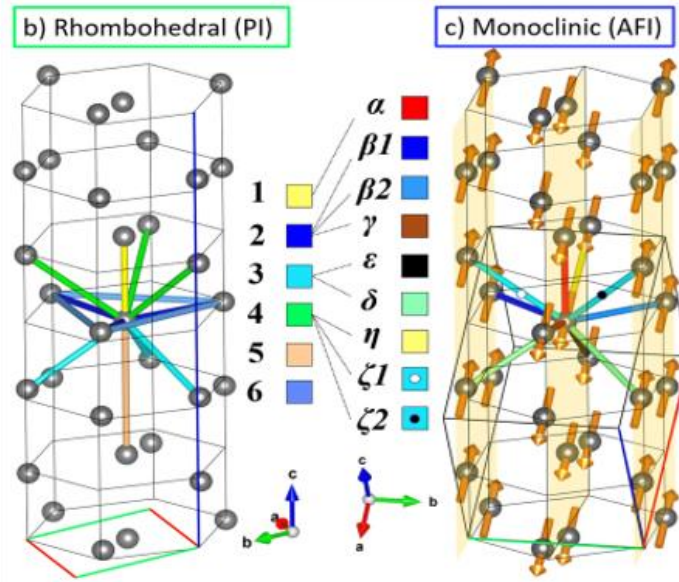


**Figure 1.2:** The figure on the left represents the visual configuration of the rhombohedral crystallographic symmetry, while the figure on the right represents the monoclinic crystallographic symmetry. Monoclinic symmetry is classified as a lower symmetry compared to rhombohedral symmetry. Source: <https://www.physik.uni-wuerzburg.de/for1162/projects/p8/>, accessed March 2019.

In addition to a change in average crystallographic symmetry,  $V_2O_3$  undergoes a change in magnetism, from being paramagnetic in the high temperature phase to antiferromagnetic in the low temperature phase. Finally,  $V_2O_3$  is a conductor in the high temperature phase, but becomes an insulator upon reaching the low temperature phase.

### 1.3 Motivation

Mott insulators represent a longstanding problem of fundamental interest to the condensed matter and materials science communities due to the rich, many-body physics originating in the strong electron correlations. In addition, they have many practical applications,

including their usage in constructing field effect transistors and other components that might be used to store internal memory. Furthermore, the Mott insulating state is thought to be the “parent state” out of which high-temperature superconductivity emerges. Thus, if we can understand the mechanism behind the Mott insulating transition, it might help the scientific community understand the principles that govern the interesting properties of higher temperature superconductors.

As a representative Mott insulator with a metal-insulator transition,  $V_2O_3$  has been the subject of significant research interest since the late 1960s. Despite this prolonged period of study, scientists are still unsure as to the detailed mechanism behind the three-fold transition that is observed in  $V_2O_3$ . A crucial question is whether the driving force for the transition originates in the lattice, magnetic, or charge degree of freedom. Careful experimental investigations that can shed light on one or more of these degrees of freedom in  $V_2O_3$  will help unravel the transition mechanism. Regarding the role played by the lattice, it has been reported that short-range correlations or distortions in the lattice from the low temperature phase persist into the high temperature phase at the transition and beyond, which would suggest that lattice dynamics play a key role in initiating the transition.

This paper will focus on the fundamental mechanism by which the metal to insulator transition (MIT) occurs. We will determine whether short-range monoclinic distortions persist into the higher temperature phase, which would imply that the lattice degree of freedom is the primary mechanism by which the MIT occurs.

## **1.4 Previous Work**

This research focuses primarily on the atomic structure of  $V_2O_3$ . I will summarize one of the published findings that was instrumental in our analysis of  $V_2O_3$ .

Pfalzer *et al.*<sup>1</sup> utilized extended x-ray absorption fine structure (EXAFS) technique to analyze  $V_2O_3$  in 2005. EXAFS is a method of absorption spectroscopy that utilizes x-rays with a narrow energy resolution to determine the absorption coefficient of a material as a function of energy<sup>2</sup>. The incident and transmitted x-ray intensities are measured as the incident x-ray energy is increased.

They reported a breaking of the triangular symmetry between neighboring vanadium atoms in the basal plane, as illustrated in Figure 1.3 below.

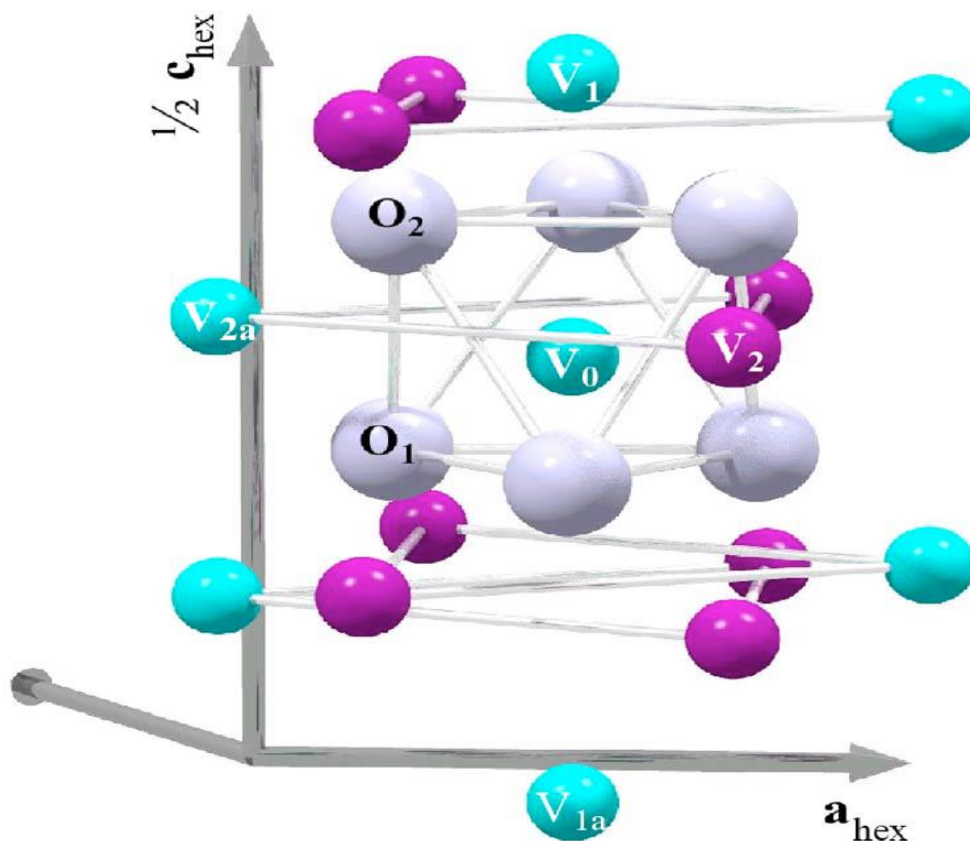


**Figure 1.3:** Pfalzer *et al.* [1] observed that the triangular symmetry between the  $V_0$  absorber atom and the  $V_{2a}$  atom was broken across the transition, and that the plane in which these atoms sit was tilted towards the c-axis.

According to Pfalzer *et al.*, the monoclinic distortion persists across the transition into the rhombohedral phase, as evidenced by the lower graph in Figure 1.4 below.

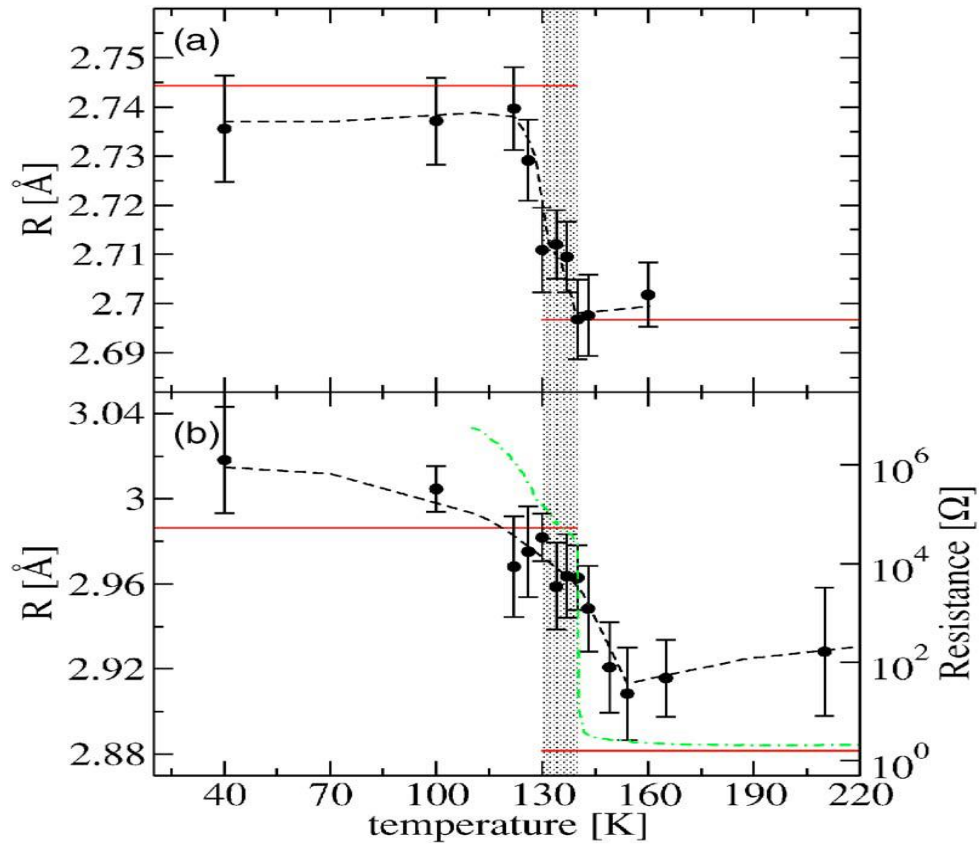


**Figure 1.4:** The lower graph from Pfalzer *et al.* [1] shows a plot of the resistivity (green) and bond lengths (black) between the neighboring vanadium atoms mentioned in Figure 1.3.

Note that this transition between the monoclinic phase and the rhombohedral phase appears to be continuous, which implies that the monoclinic distortions are persisting into the higher temperature phase. This would imply that the lattice degree of freedom is the driving force for the MIT.

## 1.5 Scientific question addressed by this research

Considering the findings proposed by Pfalzer *et al.*, we needed to determine whether or not these short-range monoclinic distortions were indeed persisting into the higher temperature

phase and understand the extent to which the lattice degree of freedom was responsible for the MIT. As there are magnetic correlations in  $V_2O_3$ , it was also important to probe the influence of the spin degree of freedom on the transition.

The results published by Pfalzer have not previously been replicated, thus we decided to shed light on their findings using pair distribution function (PDF) analysis, which will be discussed in further detail in Chapter 2.

## **1.6 Summary of results**

No local monoclinic distortions were found to persist into the higher temperature phase, which implies that the lattice degree of freedom is not the primary mechanism behind the MIT. Furthermore, antiferromagnetic correlations were too small to identify in our data, but previous inelastic neutron experiments confirm that they do exist beyond the transition, implying that the spin degree of freedom may be primarily responsible for the MIT<sup>3</sup>.

## **1.7 Overview**

Chapter 2 will discuss in great detail the methods used to obtain and analyze the data that supports the conclusions found in section 1.7. Chapter 3 will describe the analysis and discuss in greater detail the conclusions drawn in section 1.7.

# Chapter 2

## Procedural Methods

This chapter includes details of how samples were prepared and acquired, as well as details of the neutron PDF experiment.

### 2.1 Sample Acquisition and Characterization

Two different samples of  $V_2O_3$  were acquired in preparation for the neutron PDF experiment. The primary sample was prepared by Hiroshi Kageyama and Kentaro Higashi of the Department of Energy and Hydrocarbon Chemistry at Kyoto University. This sample was characterized via powder x-ray diffraction and magnetic susceptibility measurements prior to the PDF experiments, confirming the purity of the sample and the presence of the expected transition. The secondary sample was purchased commercially from Alfa-Aesar. From initial inspection of the diffraction patterns collected during the subsequent neutron PDF experiment, the commercial sample appeared to have a high level of impurities. Thus, primary focus was placed on the samples prepared by the Kageyama group.

### 2.2 Experimental Procedure and Data Collection

## 2.2.1 Experimental preparation

For the neutron PDF experiment, powder specimens of the Kageyama and commercial samples were loaded into thin quartz capillaries in an argon filled glovebox and sealed with a rubber stopper and epoxy to prevent degradation of the sample due to exposure to air. The total sample mass in each capillary was approximately 300 mg. For the x-ray PDF experiment, smaller quantities (~10 mg) were loaded into a thin Kapton capillary and sealed with clay.

Using the SNS NOMAD site<sup>4</sup>, we downloaded the PDFgui 2019-B Silicon standard fit in order to determine calibrated values for Qdamp and Qbroad. Three fitting ranges were used in the experiment. They were 30 Å, 40 Å and 50 Å. The only parameter that seemed to vary between the fits was the fitting range, shown in Table 2.2.1.

	Fitting Range		
	30 Å	40 Å	50 Å
Qdamp	0.0196766354997	0.0210848687236	0.0213301096799
Qbroad	0.0259054354956	0.0214991419291	0.0184760240622

**Table 2.2.1-** Each fitting range with the associated standard Qdamp and Qbroad values.

Once these standard values were determined, they were used for the data collection of the V<sub>2</sub>O<sub>3</sub> samples in their respective fitting ranges.

## 2.2.2 Data collection

The neutron PDF experiment was performed at Oak Ridge National Laboratory at the Spallation Neutron Source (SNS) on the NOMAD beamline in August of 2019. The Kageyama sample, the commercial sample and an empty quartz capillary were placed on the shifter that held the capillaries in place. Collecting data on the empty capillary would provide us with a

background to subtract from the data collected on the actual samples. Since  $V_2O_3$  undergoes a metal-to-insulator transition in between 140 K and 160 K, a temperature series was programmed at several temperatures below the expected transition and above the transition. This wide temperature range would ensure that the metal-to-insulator transition was included. This range also ensured that the low temperature, monoclinic symmetry and high temperature, rhombohedral symmetries were properly characterized in the data collection.

Before data was collected, the sample was cooled to 100 K from 300 K and allowed to equilibrate. For each temperature, data was collected after equilibration and allowed to increase to the next temperature, where the cycle would repeat. This was done in steps of 10 K from 100 K until a temperature of 140 K was reached. From 140 K onwards, data was collected in steps of 5 K until the temperature reached 190 K. From 190 K, data was collected in steps of 10 K until reaching 210 K. From there, data was collected in steps of 20 K until reaching 250 K. Data was then taken at 275 K, 300 K, 333 K, 367 K, and finished at 400 K. To ensure that the scattering data had a sufficiently good signal-to-noise ratio, the scattering pattern was measured for approximately 48 minutes at each temperature. The data reduction and Fourier transform were performed using the data processing scripts on the beamline computers.

The x-ray PDF experiment was performed at beamline 28-ID-1 of the National Synchrotron Light Source II (NSLS-II) at Brookhaven National Laboratory using an x-ray wavelength of 0.18 Å. The Kageyama sample was placed in a liquid helium cryostat capable of a temperature range of 5 K to 500 K. The diffraction patterns were recorded on a large area detector made of amorphous silicon and azimuthally integrated using Fit2D to obtain 1D diffraction patterns. These diffraction patterns were normalized and Fourier transformed to produce the PDF using standard data reduction protocols as implemented by the software at the

beamline. Data was taken between 4-5 K and 400 K in steps of 5 K, with approximately two minutes of data collection time per temperature point. This rapid data acquisition was enabled by the extreme intensity of the x-ray beam at NSLS-II.

## 2.3 Pair Distribution Function (PDF)

Pair distribution function (PDF) analysis is used to understand the structures of materials on nanometer or sub-nanometer length scales. This complements conventional crystallographic methods, such as x-ray diffraction, which are valuable in determining the long-range, average structure of materials. In conventional crystallography, the data is analyzed as a function of scattering angle ( $2\theta$ ), in what is called reciprocal space rather than in the familiar real space that we naturally think in. Bragg peaks, which refer to intense scattering at specific angles, contain information about the average, periodic structure of the material, and can be analyzed in reciprocal space to yield information about the crystallographic unit cell. Diffuse scattering, which refers to scattered intensity that occurs underneath or between Bragg peaks, contains information about local structural deviations from the long-range structure, which are often important for the properties of the materials. However, diffuse scattering is ignored in conventional crystallographic approaches, meaning important information about the local structure is lost. In contrast, the PDF method allows for direct insight into the local structure of a material by Fourier transforming the *total* scattering (i.e., Bragg and diffuse scattering) from reciprocal space to real space, yielding information about the local and average structure directly in real space. The two types of PDF analysis that will be utilized in this work are atomic PDF

(aPDF) and magnetic PDF (mPDF). For a more comprehensive treatment of the PDF, refer to the work of Egami and Billinge<sup>5</sup>.

### 2.3.1 Atomic PDF

The mathematical expression for calculating the atomic PDF  $G(r)$  for an arbitrary collection of atoms in a material is

$$G(r) = \frac{1}{r} \sum_{i \neq j} \frac{b_i b_j}{\langle b \rangle^2} \delta(r - r_{ij}) - 4\pi r \rho_o,$$

where the double sum runs over all of the atoms in the material,  $b_i$  and  $b_j$  represent the scattering lengths of the  $i^{\text{th}}$  and  $j^{\text{th}}$  atoms,  $\langle b \rangle$  is the average scattering length of the entire material,  $r$  is the distance represented in real space,  $r_{ij}$  is the distance between atoms  $i$  and  $j$ , and  $\rho_o$  represents the average number density of atoms. The pair distribution function essentially relates the probability of finding two atoms separated by a particular distance within a material<sup>6</sup>. This corresponds to a map of the inter-atomic distances within the material. Information gleaned from the pair distribution function allows researchers to determine the structure of the unit cell of the material, as well as account for other phenomenon such as thermal fluctuations and vibrations, amongst other important properties<sup>7</sup>.

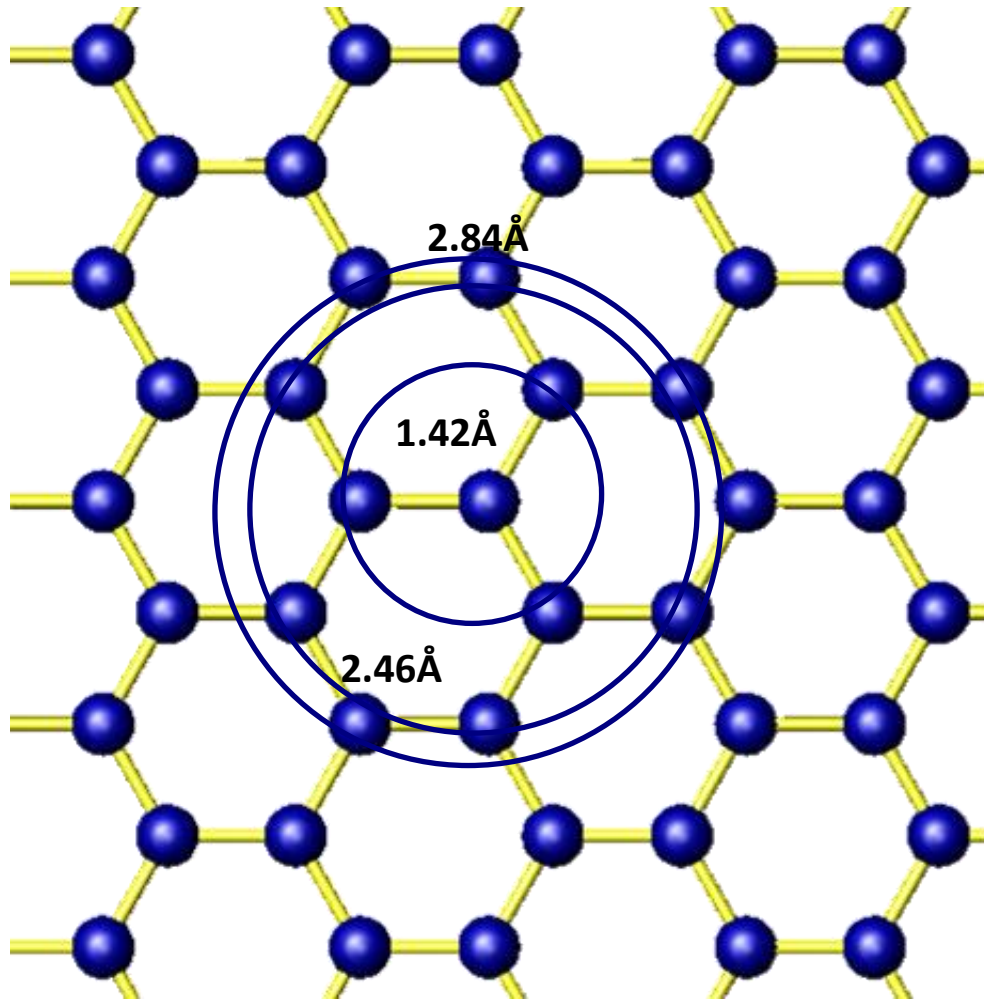


**Figure 2.1:** A one-dimensional visualization of what the pair distribution function does. Several atoms are found within various ranges of  $r$  within a certain probability. Using the range of 1.42 Å, three atoms are found within that distance.

Experimentally,  $G(r)$  is determined by way of the inverse Fourier transform of the x-ray or neutron scattering pattern. The inverse Fourier transform is given by the equation

$$G(r) = \frac{2}{\pi} \int_{Q_{min}}^{\infty} Q(S(Q) - 1) \sin(Qr) dQ,$$

where the quantity  $Q$  multiplied by  $\hbar$  gives the magnitude of the momentum transfer vector of the scattered x-rays or neutrons. As such,  $Q$  has dimensions of inverse length. On the other hand,  $S(Q)$  is dimensionless and represents the normalized, total scattering intensity. The mathematical model for  $G(r)$  is utilized to compute a structural model of the material. This is then compared to

the experimental PDF, and then refined until it provides the best possible fit to the experimental data. The advantage of PDF method, as mentioned above, is that not only is the average structure obtained by the inclusion of Bragg diffraction in the Fourier transform, but also the diffuse scattering which contains information about the local structure, which can deviate significantly from the average structure<sup>8</sup>. The location of peaks determined by the inverse Fourier transform provide insight as to the distances by which atoms are most probably separated. Since  $V_2O_3$  undergoes a metal-to-insulator transition in addition to a change in crystallographic symmetry as well as a change in magnetic properties, PDF is an appropriate method of investigation of this material, particularly to investigate the claims of local structural distortions persisting above the metal-insulator transition.

### **2.3.2 Magnetic pair distribution function (mPDF) analysis**

Neutron scattering data not only provides us with viable data for aPDF analysis, but is also useful for determining the spatial separation and the relative magnetic orientation of magnetic moments resulting from unpaired electron spins in a material<sup>8</sup>. Neutron scattering data allows us to determine these quantities because, as a spin-1/2 quantum particle, a neutron has an intrinsic magnetic moment<sup>9</sup>, and therefore interacts with magnetic fields inside of a material. At the same time, neutrons are not subject to Coulomb forces due to their lack of electric charge, so the only interaction a neutron can have with an electron is magnetic. Thus, neutrons are the perfect candidates for capturing data related to magnetic structure in materials. mPDF analysis is therefore performed using neutron scattering data. mPDF analysis of x-ray scattering data is not feasible due to the relatively weak interaction between x-rays and spins.

The mPDF  $d(r)$  from a collection of spin-only magnetic moments can be quantified using the formula

$$d(r) = \left( \frac{3}{N_s 2S(S+1)} \sum_{i \neq j} \left[ \frac{A_{ij}}{r} \delta(r - r_{ij}) + B_{ij} \frac{r}{r_{ij}^3} \theta(r_{ij} - r) \right] - \frac{2}{3} \langle m \rangle r \right) * \mathcal{M} + d_{para},$$

where  $N_s$  is the number of moments,  $S$  is the spin quantum number,  $r_{ij}$  is the distance between moments  $i$  and  $j$ ,  $A_{ij}$  and  $B_{ij}$  encode the spin-spin correlations transverse and parallel to the vector  $\mathbf{r}_{ij}$ ,  $\langle m \rangle$  is the net magnetization density,  $*$  is the convolution operator,  $\mathcal{M}$  is the real-space spin density distribution of the individual magnetic moments, and  $d_{para}$  is the contribution from individual moments that is independent of any spin-spin correlations and results only in a peak at very low  $r$  values<sup>10</sup>.

Experimentally, the mPDF is the inverse Fourier transform of the intensity of neutrons scattered from the magnetic moments in the material instead of the nuclei. When data is collected using neutron scattering, the combined scattering pattern is a combination of both the aPDF signals and mPDF signals such that  $G(r) + d(r)$  equals the total PDF pattern. However, nuclei typically have a higher scattering strength compared to magnetic moments. Thus, the mPDF  $d(r)$  can be many times smaller than the atomic PDF  $G(r)$ . A Fourier filter is applied to the data to filter out high frequency noise which might otherwise obscure the mPDF signal. For  $V_2O_3$ , a temperature filter was also applied, as we did not expect a signal in the high temperature regime.

Two important parameters when refining an mPDF signal are the ordered scale factor and the damping factor. The ordered scale factor describes how strongly the magnetic moments keep a definite orientation relative to one another. As the magnitude of the ordered scale factor increases, the more correlated the magnetic moments become. The damping factor quantifies how much the magnetic signal strength decreases in proportion to distance due to finite

correlation length. In the limit of infinitely long-range magnetic correlations, the damping factor converges to zero, and the mPDF will remain undamped over very long distances.

## **2.4 Data Analysis**

Various software packages were used in the analysis of the data collected. The graphical program PDFgui was utilized to determine the viability of the raw data collected during the experiment and characterize the fits. Once the viability of the data was determined to be sound, the data was imported into a diffpy environment which also performed PDF fits. The diffpy method helped overcome some of the shortcomings of PDFGui, which will be discussed in a subsequent section. Magnetic PDF (mPDF) analysis was performed using the diffPy.mpdf package.

### **2.4.1 PDFgui**

The open-source program PDFgui<sup>11</sup> was developed for the express purpose of easily calculating the atomic PDF and refining structural models using experimental PDF data. The refined parameters relate to the structure of the material, such as the unit cell dimensions and positions of atoms within the unit cell, and are used to perform a least-squares fit to the experimental data.

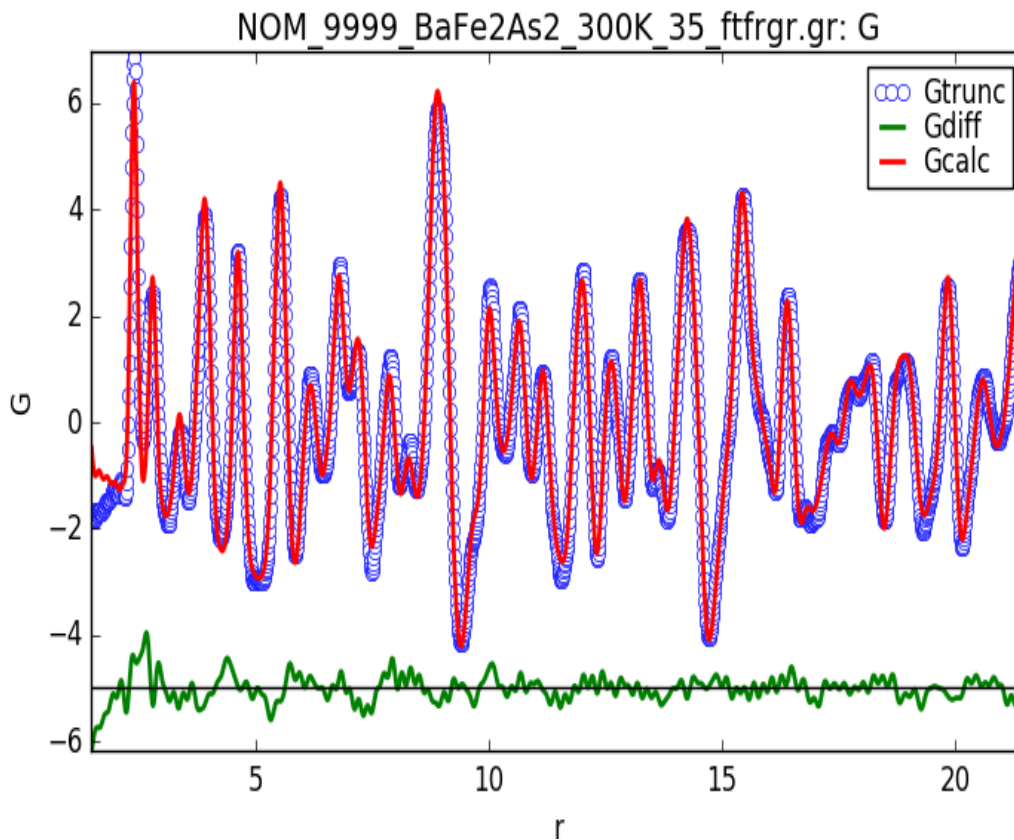


**Figure 2.2:** A sample PDF fit, where the blue dots represent the experimental data, the red line represents the actual fit, and the green line represents the difference between the data and the fit.

It is important to consider that the method of refinement depends on the material. Simpler materials will require fewer parameters, so the refinement will be easier. More complicated materials, such as  $V_2O_3$ , require more complex refinements with more involved fitting strategies, such as carefully selecting the order of the refinement of parameters. PDFgui is limited in its ability to provide high quality refinements for more complex materials and refinements. Thus, in the case of  $V_2O_3$  it was used to characterize the data initially, but not to perform the final analysis. Refinements used in the final data analysis were performed using python packages included in the DiffPy library that has been developed for PDF data analysis.

## 2.4.2 PDF Refinement in diffPy

Using the diffPy<sup>12</sup> environment to perform the PDF refinements makes it possible to perform a large quantity of these refinements without having to manually produce them. Various parameters such as the fitting range could be varied and numerous fits produced in the span of days, while performing such a large quantity of refinements in PDFgui would have taken weeks or even months. The code used to perform these fits is easily modified for other materials. Instead of manually determining the order of refinement of the parameters, the software addresses it intrinsically, and will optimize the parameters without human guidance or intervention.

## 2.4.3 Shortcomings of PDFgui and diffPy

PDFgui and diffPy have disadvantages and weaknesses. Sometimes, the refinement parameters will converge to unphysical values. For example, the atomic displacement parameters representing vibrational motion of the atoms sometimes converge to extremely high values or negative values, both of which represent unphysical motion.

A challenge particular to PDFgui (and not unheard of when using the diffPy environment) occurs when fitting parameters stop improving despite the relative quality of the fit being poor. This indicates there is room for further optimization, yet the lack of improvement on the local level prevents further optimization. This is usually due to a lack of suitable initial conditions or unrealistic initial values for certain parameters like the ADPs or lattice parameters. This problem is usually amended by changing the initial conditions or values and can be done until the fit begins to optimize again.

## 2.4.4 diffPy.mpdf Package

A different software package is required to perform mPDF analysis. The diffPy.mpdf<sup>13</sup> package is a Python package that can calculate the mPDF from magnetic structures. The process begins by specifying a diffpy.structure object, the magnetic propagation vectors, and the magnetic basis vectors. Once these are specified, the user can generate magnetic configurations and calculate the mPDF. Once the mPDF has been calculated, the user can perform a fit by refining the parameters described in section 2.3.2.

Not all of the information obtained in the fit residual is of interest to us. We can apply certain filters such as temperature subtraction and data smoothing to remove unnecessary information from the data so as to highlight phenomenon that are of interest. These methods help us to isolate the mPDF signal, which is significantly smaller than the atomic PDF signal.

In  $V_2O_3$ , we expect antiferromagnetic correlations to be present below the transition. Since we do not expect strong antiferromagnetic correlations to be present at temperatures far above the transition, we can apply a temperature filter to the data to subtract out any temperature-independent noise from the signal. This makes the antiferromagnetic signal more apparent.

Data smoothing can further clean up the data. Since magnetic scattering occurs at low  $Q$ , all neutron data beyond a certain limit (usually  $8 \text{ \AA}^{-1}$ ) can be left out of the inverse Fourier transform without negatively impacting the magnetic signal. This Fourier filter essentially filters out high frequencies that can obscure the signal, as well as other non-necessary signals related to the atomic structure. This data smoothing is performed within diffPy.mpdf. This filter is applied as a convolution with the sinc function in real space, which is equivalent to a step-function cutoff in  $Q$ -space.

## 2.4.5 Shortcomings of diffPy.mpdf

The fitting parameters described in Section 2.3.2 can sometimes refine to non-physical values. For example, the ordered scale factor could refine to a negative value. This negative value would suggest the material does not have physically permissible magnetic correlations.

Moreover, the damping factor can refine to a negative value. This would imply that the magnetic signal is increasing with distance, rather than decreasing, which violates basic laws of magnetostatics.

Finally, the fits can refine to poor quality if the user specified inaccurate initial conditions. This situation can be remedied by varying the initial conditions until the resulting fit is of high quality and all refinement parameters are physically acceptable.

# Chapter 3

## Results and Conclusions

### 3.1 V<sub>2</sub>O<sub>3</sub> Results and Analysis

This section will outline both the results of the atomic PDF and magnetic PDF analyses of V<sub>2</sub>O<sub>3</sub>. A qualitative discussion of the results will shed light on the mechanism behind the metal-to-insulator transition observed in V<sub>2</sub>O<sub>3</sub>, including the behavior of vanadium-vanadium bond lengths as a function of temperature as the transition is approached and surpassed. Figures will be used extensively to illustrate the lack of monoclinic distortions persisting into the high temperature phase, as well as illustrate the power of the pair distribution function. Our results indicate that there are no monoclinic distortions that persist into the high temperature phase, implying that the lattice degree of freedom is not the primary mechanism behind the MIT.

#### 3.1.1 Atomic PDF Fit Results

As described earlier, V<sub>2</sub>O<sub>3</sub> undergoes a transition in crystallographic symmetry across the metal-to-insulator transition, from low temperature monoclinic to high temperature rhombohedral. Thus, it was necessary to perform two separate sets of fits on the data, one for each structural model, to demonstrate the strength of the monoclinic fits at low temperature and the strength of the rhombohedral fits at temperatures beyond the transition.

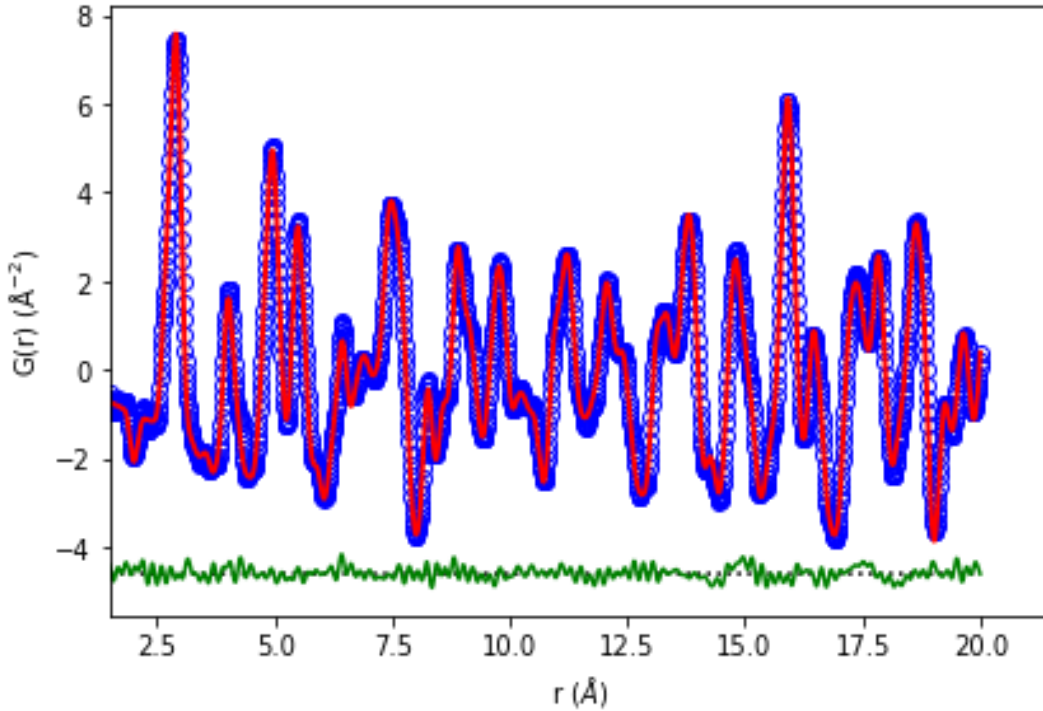


**Figure 3.1:** An atomic PDF rhombohedral neutron data plot at 300 K from 1.5 Å to 21.5Å. The red represents the actual fit, the blue dots represent the experimental data points, and the green line represents the difference between the experimental data and the fit. This is called the fit residual.

Figure 3.1 shows the neutron atomic PDF at 300 K, above the metal-insulator transition. By observation, it is clear that the fit corresponds to the data nearly point by point, which demonstrates the accuracy of the rhombohedral model at a temperature above the transition. Consequently, the fit residual is nearly flat, implying that the difference between the data and fit are very small, again affirming the accuracy of the rhombohedral model for this temperature.

The corresponding x-ray fit shown in Figure 3.2 also demonstrates the same characteristics as Figure 3.1, namely that the fit corresponds well to the data with minimal residual between the data and the calculated fit across the same fitting range.

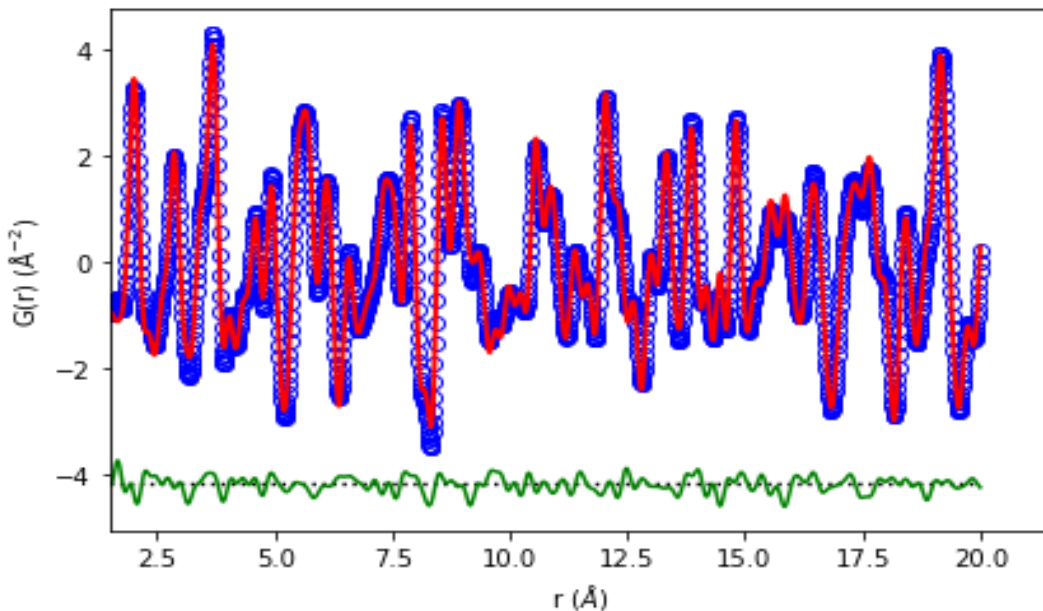


**Figure 3.2:** Atomic PDF x-ray rhombohedral fit at 303.84 K. Again, the red line represents the actual PDF fit, the blue dots represent the experimental data points, and the green represents the fit residual.

The x-ray and neutron data for the rhombohedral fits corroborate each other: at higher temperatures, the average and local structure of  $V_2O_3$  correspond to a rhombohedral crystallographic symmetry.

At low temperatures, we would expect the average crystallographic symmetry to be monoclinic. This is corroborated by low temperature neutron and x-ray atomic PDF fits. Figure 3.3 demonstrates yet again that the x-ray and neutron data corroborate each other. The fits using the monoclinic structural model adequately describe the experimental data. There are no significant fluctuations in the fit residual across the average structure. Thus, the monoclinic crystallographic symmetry aptly describes both the average and local structure of  $V_2O_3$  at low temperatures.

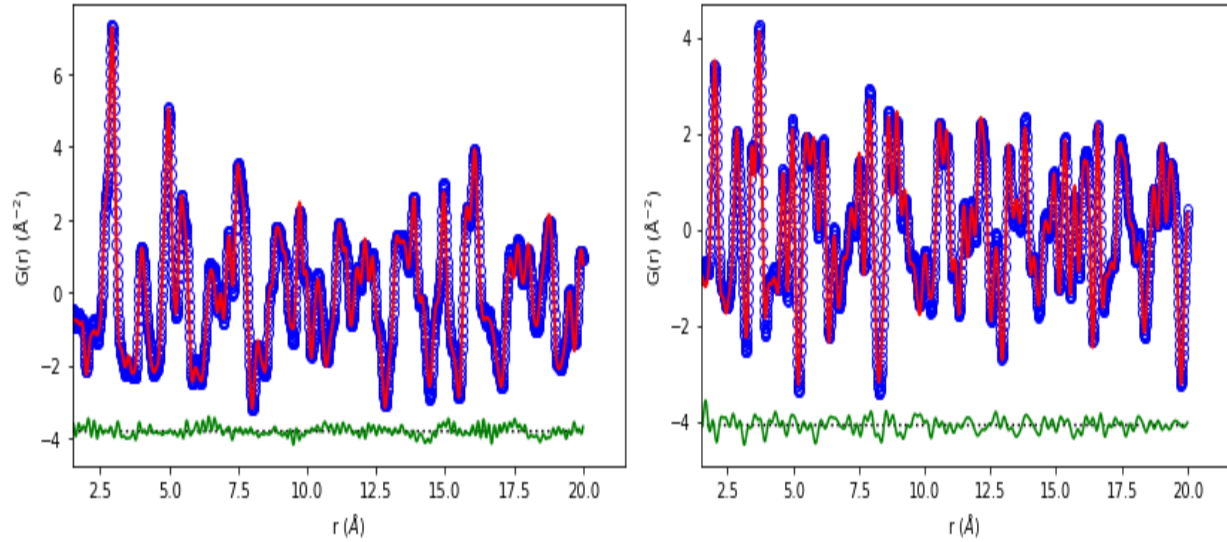


**Figure 3.3:** From left to right, an atomic PDF neutron monoclinic fit at 100 K and an atomic PDF x-ray monoclinic fit at 100.59 K. Both span ranges from 1.5 Å to 21.5 Å.

In many materials with a structural phase transition, remnants of the low-temperature structure persist into the high-temperature phase in the form of local structural correlations exhibiting the low-temperature symmetry on short length scales. This type of local structural distortion, if present, can often be observed in the PDF. With this in mind, one might expect that as  $V_2O_3$  approaches the transition temperature ( $\sim 155$  K) and beyond, the short-range structural correlations may preserve the distorted monoclinic symmetry, even as the average structure transitions to the rhombohedral symmetry on long length scales. As discussed in Chapter 1, previous analysis of  $V_2O_3$  by Pfalzer *et al.* seems to suggest that this is the case. This type of behavior would indicate that a structural precursor to the low-temperature state forms in the high-temperature phase, suggesting that the lattice degree of freedom would be primarily responsible for the metal-to-insulator transition.

Experimental evidence provided by PDF analysis does not corroborate the conclusions drawn by Pfalzer. This analysis was performed by examining fits spanning an 80 K range, from 40 K below the transition, to 40 K above the transition. We note that this analysis was mostly

performed on the x-ray data, as the work done by Pfalzer et al was performed using x-ray techniques as well. X-rays are more sensitive to the vanadium locations in the structure compared to neutrons. Thus, x-ray scattering was more useful in analyzing the vanadium-vanadium correlations than neutron scattering.

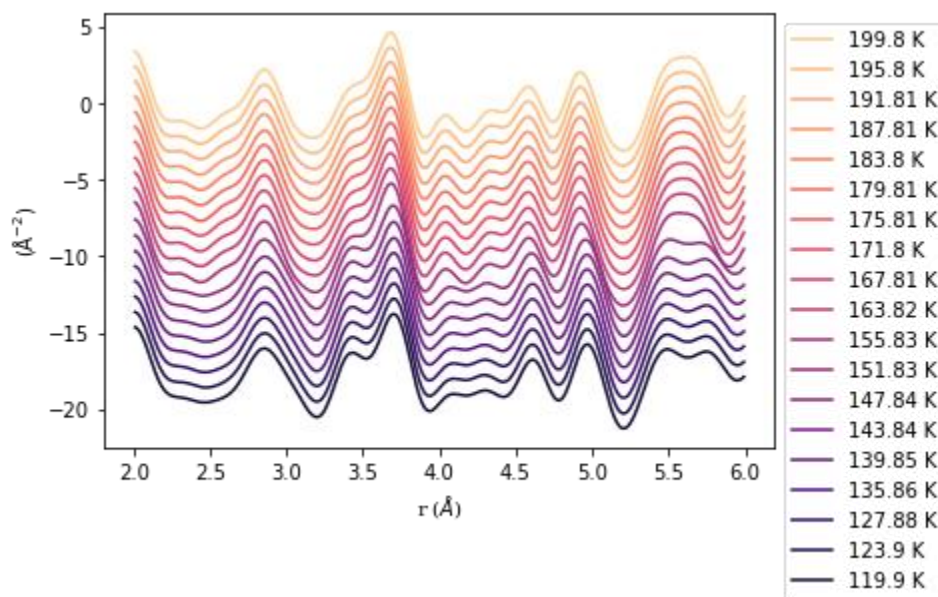


**Figure 3.4:** Plot of various atomic PDF x-ray data sets as a temperature series. Many features of note were found between the distances of 2.0 Å and 6.0 Å, which corresponds to the local structure.

Figure 3.4 shows the low- $r$  region of the x-ray PDF data at several temperatures spanning the transition. Looking closely at the temperatures corresponding to 147.84 K to 155.83 K, the PDF curves do not appear to transition smoothly. In contrast, the transition from the low temperature, monoclinic crystallographic symmetry appears to transition abruptly to the rhombohedral crystallographic symmetry, based on the notable change of shape in the PDF curves. Of particular note are the features found between 2.0 Å and 2.8 Å and the features between 4.0 Å and 4.5 Å. Figure 3.5 below provides a close-up view of the features described between these two ranges.

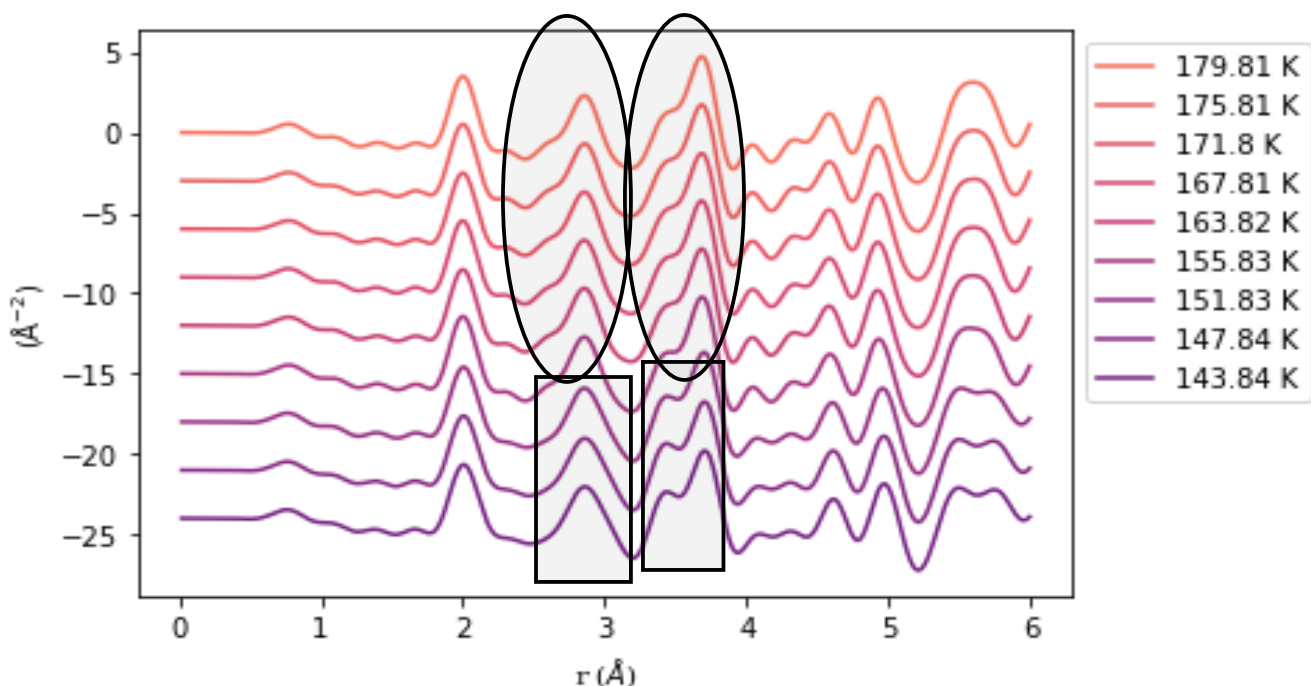


**Figure 3.5:** A close-up view of the aforementioned features. The rectangles represent monoclinic distortions present in the temperatures below the transition. The ovals represent features present in the rhombohedral, high temperature phase above and during the transition.

Specifically, the monoclinic features in the 2.5 Å to 3.0 Å range represent very broad peaks in the pattern. Once the transition is reached, however, the structure immediately takes on features that correspond to a rhombohedral crystallographic symmetry. These features include a distinct shoulder suddenly emerging on the left tail of the peaks, and a decrease in the broadness of the corresponding peaks. A similar pattern of features is found in the 3.0 Å to 4.0 Å range. In the rectangular portion corresponding to this range, the peaks are characterized as doublets, two distinct peaks that correspond to two closely correlated atoms. Once the transition is reached (the rectangular region), these doublets seem to merge abruptly into a single peak characterized by a shoulder on the left tail. This pattern of distinct features is prominent across the full range of  $r$ , including the low- $r$  region shown here. The data then indicates that no low-temperature vanadium distortions persist into the high temperature phase. Thus, our PDF evidence clearly demonstrates that the transition is abrupt rather than smooth, in contrast to the earlier result by

Pfalzer *et al.* Moreover, this abruptness occurs even on the local level, suggesting that the mechanism behind the metal-to-insulator transition is significantly impacted by abrupt changes to the local structure.

Atomic PDF using neutron scattering provides strong evidence corroborating the idea of an abrupt transition in the local structure as well as the average structure. The neutron PDF differs from the x-ray PDF in that it is more sensitive to the oxygen locations in the structure, as vanadium atoms have a very small scattering length for neutrons. Figures 3.6 and 3.7 display representative neutron PDF data sets across the transition.

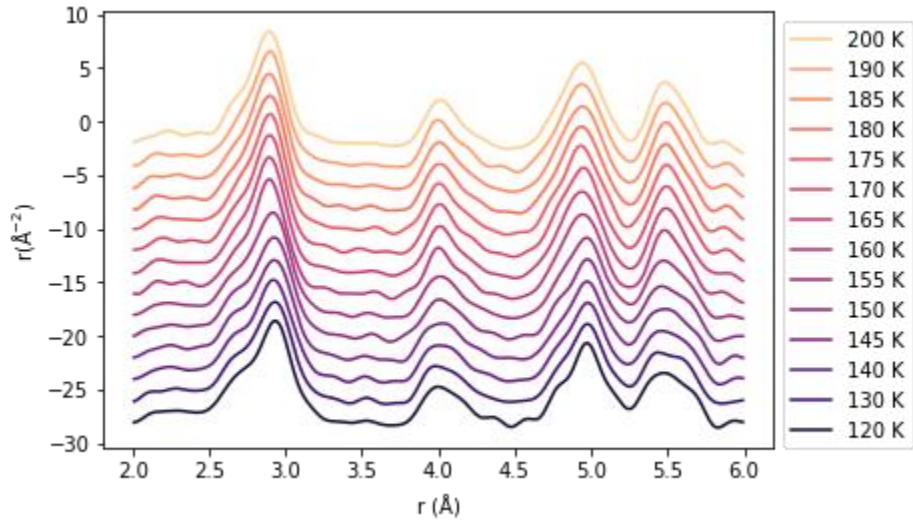


**Figure 3.6:** Corresponding atomic PDF data by neutron scattering across an 80 K temperature range.

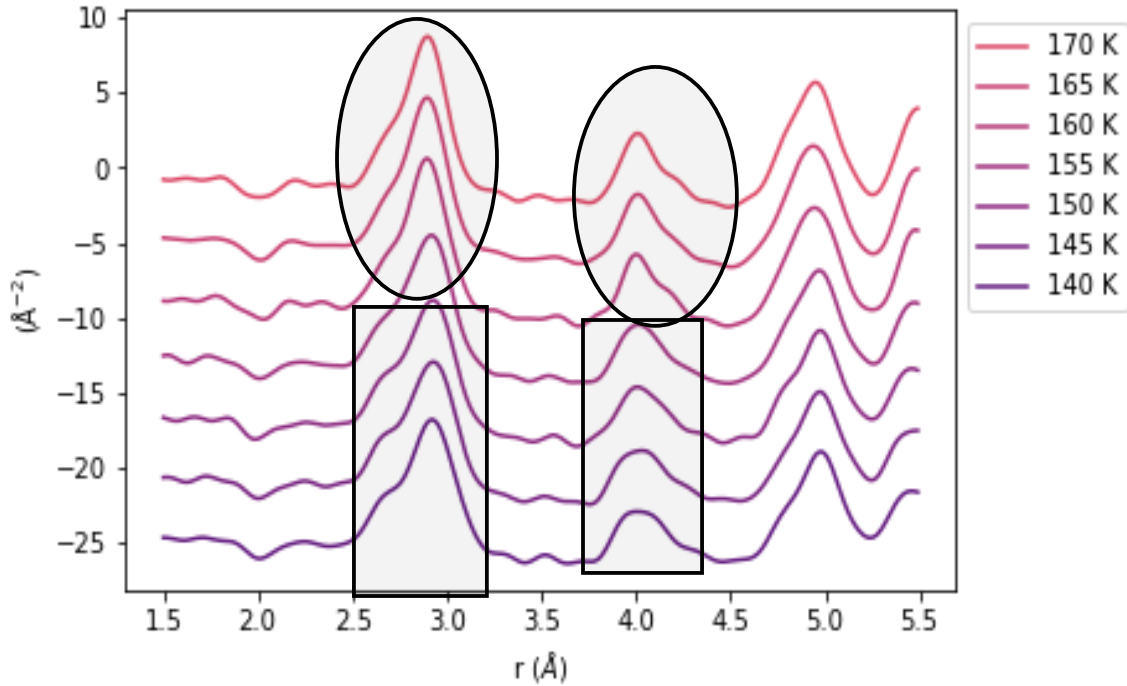


**Figure 3.7:** A closer look at the neutron data sets from figure 6 reveals that the rhombohedral features found in the circular regions are significantly distinct from the monoclinic features found in the rectangular regions.

A closer look at these data sets demonstrates that across the same  $r$  ranges as the x-ray plots, we can see distinct features as the material transitions from one phase to the other. The monoclinic features (rectangular region) found between 2.5 Å and 3.2 Å are characterized by a single peak that contains a distinct shoulder on the left tail, while the rhombohedral features (oval region) are characterized by a significantly narrower peak where the left tail shoulder becomes abruptly less prominent as the temperature rises. Between 3.7 Å and 4.3 Å, the monoclinic features are characterized by a small but very broad peak, while the rhombohedral features are characterized by a significantly narrower peak characterized by a shoulder on the right tail. As evidenced by these features, the transition from monoclinic to rhombohedral crystallographic symmetry is extremely abrupt. No low temperature oxygen distortions persist into the high temperature phase in the neutron scattering data. This again suggests that the lattice

shows no tendency toward the insulating monoclinic structure when in the high-temperature rhombohedral phase, making it unlikely that the lattice degree of freedom is the driving force behind the metal-to-insulator transition in  $V_2O_3$ .

If no monoclinic distortions persist into the high-temperature phase, as the results thus far have suggested, then the behavior of the vanadium-vanadium bond lengths will be a telling indicator. The vanadium-vanadium bond lengths will be different for the monoclinic, low temperature phase when compared to the bond lengths in the rhombohedral, high temperature phase. Having already established that this transition occurs abruptly, we would expect the behavior of the monoclinic model bond lengths at the transition and beyond to exhibit the same behavior as the rhombohedral model bond lengths. In other words, the monoclinic model bond lengths should converge into the rhombohedral model bond lengths. Figures 3.8 and 3.9 illustrate this.

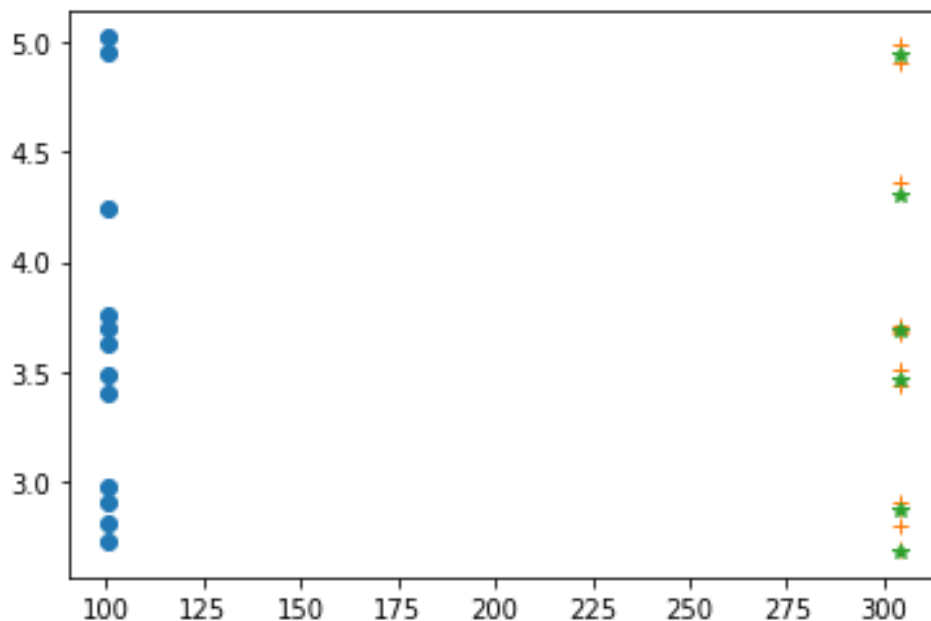


**Figure 3.8:** Plotted above are the bond lengths corresponding to the monoclinic model at low temperature (blue dots), as well as both the monoclinic and rhombohedral vanadium bond lengths at the highest temperature. The orange plus signs represent the high temperature monoclinic bond lengths and the green stars represent the high temperature rhombohedral bond lengths as a function of temperature in kelvin and bond length in angstroms.

Note that there are twelve distinct bond lengths corresponding to the low temperature monoclinic model. At high temperatures, there are six distinct bond lengths corresponding to the high temperature rhombohedral model. Convergence of the monoclinic model to the rhombohedral model would be visualized as those twelve distinct bond lengths converging on or near the rhombohedral bond lengths. Indeed, by inspection at 300 K, the monoclinic bond lengths do appear to converge into what would be expected from the rhombohedral model.

However, it is important to establish that this behavior also occurs near the transition. Using these bond lengths, we can demonstrate the convergence of the monoclinic phase into the rhombohedral phase.

When comparing the monoclinic bond lengths at 150 K to those at 100 K, it appears the bond lengths have converged significantly. Moreover, they appear to converge towards the

expected rhombohedral bond lengths. This behavior at the transition further evidences the abruptness of the transition, which is supported by the data in Figure 3.9.

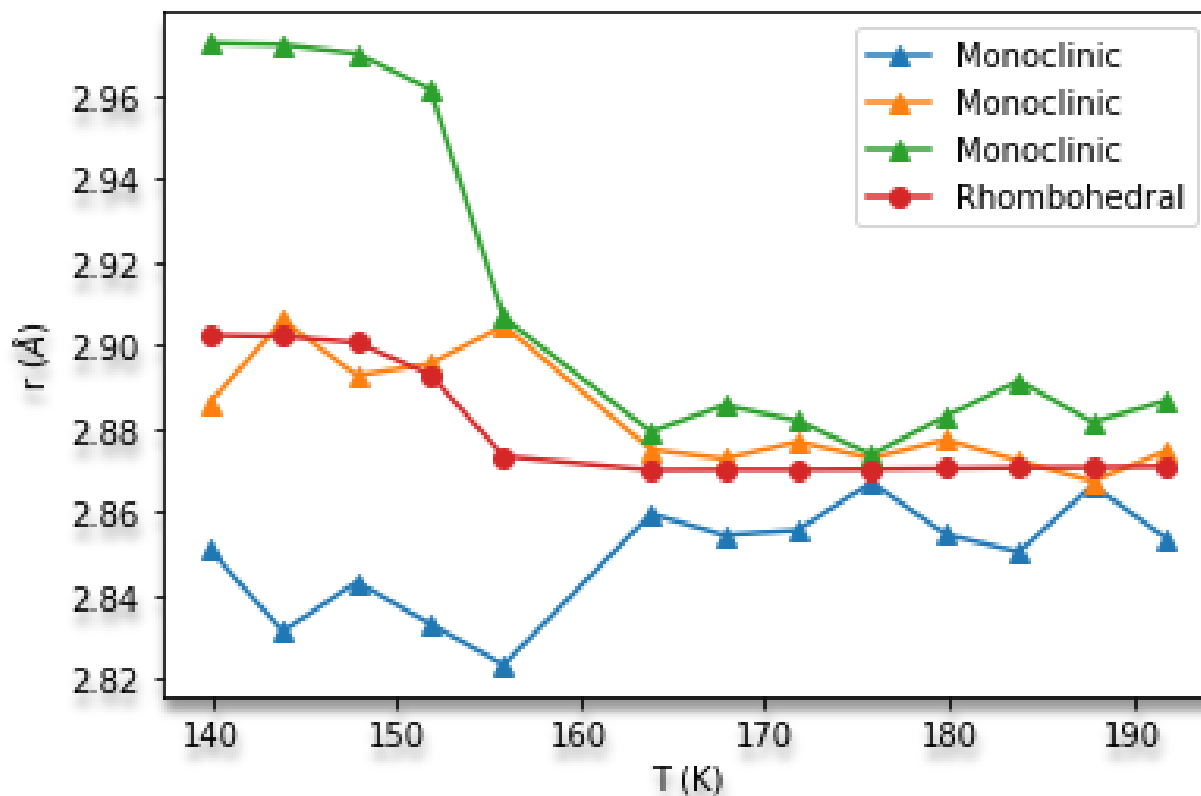


**Figure 3.9:** Here we depict a close-up view of how the monoclinic phase converges into the rhombohedral phase. The green, orange, and blue lines represent the three distinct monoclinic bond lengths found below the transition, while the red line represents the rhombohedral phase bond lengths.

Clearly the monoclinic phase bond lengths converge into the rhombohedral phase at the transition and beyond in an abrupt manner, once again ruling out the possibility of any short-range monoclinic distortions in the local structure above the transition.

### 3.1.2 Magnetic PDF Analysis

Atomic PDF results suggest that the lattice degree of freedom is not responsible for the MIT observed in  $V_2O_3$ . Thus, as discussed in Chapter 1, another possible mechanism is the spin degree of freedom. Assuming this is the case, we would expect to see antiferromagnetic correlations corresponding to the low temperature phase to persist above the transition into the high temperature phase. As discussed in Chapter 2, this phenomenon can be observed using mPDF analysis.

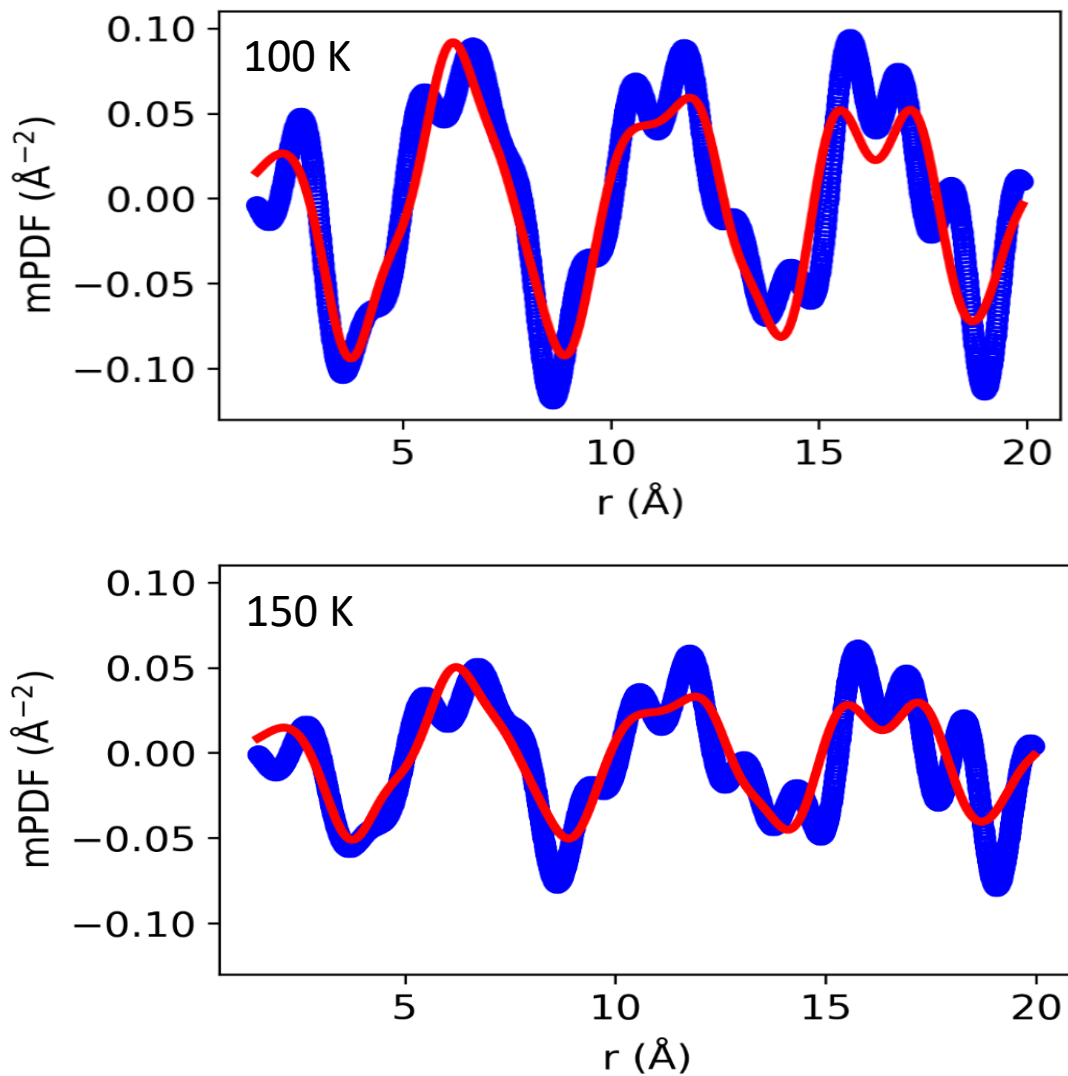


**Figure 3.10:** This figure shows two mPDF fits to the data at 100 K and 150 K respectively. The red line represents the fit, while the blue line represents the experimental data.

Figure 3.10 demonstrates that at low temperature, the magnetic structure is indeed antiferromagnetic, due to the fact that the fits, which assume an antiferromagnetic structure, align very well with the experimental data. Figure 3.10 also demonstrates that, as expected, there is a temperature evolution of the magnetism when approaching the transition. The amplitude of the antiferromagnetic correlations significantly decreases as we near the transition. Figure 3.11 below depicts this magnetic evolution.

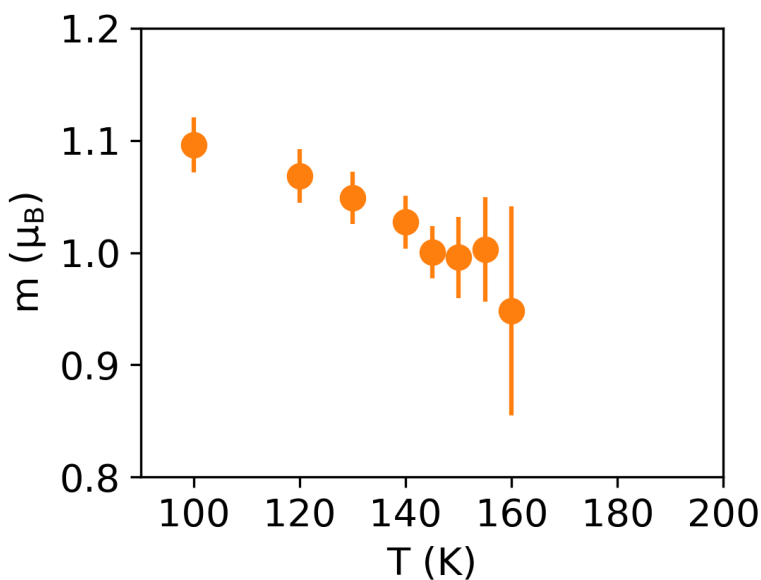


**Figure 3.11:** This figure demonstrates the best fit ordered moment in units of the Bohr magneton as a function of temperature. The orange dots are proportional to the square root of the amplitude of the mPDF fit. Note how it decreases as we approach the transition.

Figure 3.11 demonstrates that the magnetic order does not decrease continuously to zero as we approach the transition. Therefore, this transition is a first order transition.

Unfortunately, the signal produced by possible high temperature antiferromagnetic fluctuations persisting across the transition was too small and weak to be seen in our data.

However, previous inelastic neutron scattering experiments suggest that these antiferromagnetic

correlations do exist in the high temperature phase, suggesting that the spin degree of freedom may be primarily responsible for the MIT<sup>14</sup>.

### 3.1.3 Analysis of V<sub>2</sub>O<sub>3</sub> Results

Analysis of various PDF data sets over a temperature range that include the transition establish that no monoclinic distortions persist beyond the transition, refuting conclusions drawn from earlier work done on V<sub>2</sub>O<sub>3</sub>. This is further corroborated by analyzing the bond lengths of the monoclinic model as a function of temperature and comparison to the bond lengths in the rhombohedral model and noting the convergence of the monoclinic model to the rhombohedral model at the transition and beyond. We speculate that the discrepancy between the current results and the earlier results by Pfalzer *et al.* may be due to sample quality. The sample used in the earlier study showed a transition at a significantly lower temperature (130 – 140 K), likely due to defects and vacancies in the crystal structure. These defects could easily influence the data and structure in such a way as to make it seem that low-temperature monoclinic distortions persist to higher temperatures.

## 3.2 Future Work

Since we now understand that the role of the lattice degree of freedom is a secondary factor in the metal-to-insulator transition, future efforts can focus on analyzing the role of the spin degree of freedom on the system utilizing mPDF. Further mPDF analysis will be essential to unraveling the magnetic mysteries of V<sub>2</sub>O<sub>3</sub>.

### 3.3 Summary and Conclusion

The results obtained by experiment and analysis on  $V_2O_3$  have further served to demonstrate how significant local distortions and changes to local symmetry are to understanding the complex behavior exhibited by quantum systems like  $V_2O_3$ . Understanding the secondary role of the lattice degree of freedom in this system will allow us to turn our attention to other potential primary mechanisms, such as the spin degree of freedom, thus opening more avenues to understand Mott insulators in general.

# Bibliography

1. P. Pfalzer, G. Obermeier, M. Klemm, and S. Horn, 2005, „Structural precursor to the metal-insulator transition in  $V_2O_3$ ”, DOI: 10.1103/PhysRevB.73.144106
2. M. Newville, B. Ravel, D. Haskel, J.J. Rehra, E.A. Stern, Y. Yacoby, “Analysis of multiple scattering XAFS data using theoretical standards”, *Physica B* 208 & 209 (1995)
3. Ethan Fletcher, Benjamin Frandsen, Hiroshi Kageyama et. al., “Clarifying the role of the lattice degree of freedom in the canonical metal to insulator transition in  $V_2O_3$ ”, will be submitted to *Physical Review B* in mid-2021.
4. <https://www.sciencedirect.com/science/article/pii/S0168583X12003291>
5. T. Egami and S.J.L. Billinge, *Underneath the Bragg Peaks: Structural Analysis of Complex Materials* (Elsevier, Amsterdam, 2012).
6. [https://en.wikipedia.org/wiki/Pair\\_distribution\\_function](https://en.wikipedia.org/wiki/Pair_distribution_function), accessed March 2021
7. T. Proffen, S.J.L. Billinge, T. Egami, and D. Louca, “Structural analysis of complex materials using the atomic pair distribution function – a practical guide”, *Zeitschrift Fur Kristallographie-Crystalline Materials* **218**, (2003).
8. B.A. Frandsen, X. Yang, and S.J.L. Billinge, “Magnetic pair distribution function analysis of local magnetic correlations”, *Acta Crystallographica Section A Foundations and Advances* **70**, 3 (2013).
9. Gell, Y.; Lichtenberg, D.B. (1969). "Quark model and the magnetic moments of proton and neutron". *Il Nuovo Cimento A. Series 10*. **61** (1): 27-40. [Bibcode:1969NCimA..61...27G, doi:10.1007/BF02760010, S2CID 123822660](https://doi.org/10.1007/BF02760010).
10. B.A. Frandsen and S.J.L. Billinge, “Magnetic structure determination from the magnetic pair distribution function (mPDF): ground state of  $MnO$ ”, *Acta Crystallographica Section A Foundations and Advances* **71**, 325 (2015).
11. C.L. Farrow, P. Juhás, J.W. Liu, D. Bryndin, E.S. Božin, J. Bloch, Th. Proffen and S.J.L. Billinge, “PDFfit2 and PDFgui: computer programs for studying nanostructures in crystals”, *J. Phys.: Condens. Matter* **19**, 335219 (2007)
12. DiffPy-CMI <http://dx.doi.org/10.1107/S2053273315014473>
13. <https://github.com/benfrandsen/diffpy.magpdf>
14. Wei Bao, C. Broholm, G. Aeppli, S. A. Carter, P. Dai, T. F. Rosenbaum, J. M. Honig, P. Metcalf, and S. F. Trevino, “Magnetic correlations and quantum criticality in the insulating antiferromagnetic, insulating spin liquid, renormalized Fermi liquid, and metallic antiferromagnetic phases of the Mott system  $V_2O_3$ ”, *Phys. Rev. B* **58**, 12727 (1998)